Excited-State Dynamics of Er3+ in Gd2O3 Nanocrystals

ARTICLE *in* THE JOURNAL OF PHYSICAL CHEMISTRY C · JUNE 2007

Impact Factor: 4.77 · DOI: 10.1021/jp066223e

4 AUTHORS, INCLUDING:

G. K. Liu
Argonne National Laboratory
162 PUBLICATIONS **2,595** CITATIONS

SEE PROFILE

ARTICLES

Excited-State Dynamics of Er^{3+} in Gd_2O_3 Nanocrystals

Xueyuan Chen,*,† En Ma,† Guokui Liu,‡ and Min Yin§

State Key Laboratory of Structural Chemistry, National Engineering Research Center for Optoelectronic Crystalline Materials, Fujian Institute of Research on the Structure of Matter, Chinese Academy of Sciences, Fuzhou, Fujian 350002, China, Chemistry Division, Argonne National Laboratory, Argonne, Illinois 60439, U.S.A., and Department of Physics, University of Science and Technology of China, Hefei, Anhui 230026, China

Received: September 22, 2006; In Final Form: February 25, 2007

The temperature-dependent lifetime of the green emission from Er^{3+} ions in 40−50 nm Gd_2O_3 nanocrystals has been measured and analyzed. The luminescence decay from the $^4S_{3/2}$ state of Er^{3+} shows nonexponential characteristics when excited directly to the thermally coupled $^2H_{11/2}$ from 10 to 300 K, indicating energy transfer to defects in the nanocrystals. The intrinsic lifetime of the $^4S_{3/2}$ state was determined by utilizing the efficient energy transfer from Gd^{3+} to Er^{3+}. It is shown that, on the basis of a simplified thermalization model, multiphonon nonradiative relaxation from $^4S_{3/2}$ to $^4F_{9/2}$ plays a leading role in the observed temperature dependence of the intrinsic lifetime. Furthermore, a reciprocity method has been successfully extended to the calculation of the room-temperature emission spectrum of the $^2H_{11/2}-^4I_{15/2}$ transition according to the measured excitation spectrum. Unusual phonon side bands in the laser excitation spectrum are observed in the hypersensitive transitions of Er^{3+}. The origin of the phonon side bands is ascribed to the M process that involves the infrared-active lattice modes.

1. Introduction

Since the rapid advances in nanotechnologies, particularly, the development of new methods for materials synthesis, there has been growing interest in studying the optical behavior of rare-earth (RE) ions in nanomaterials.[1−3] RE-doped inorganic nanophosphor is one of the most promising materials for a variety of applications in solid-state lasers, lighting and displays, and biolabels.[3,4] The Gd_2O_3 microcrystals doped with Eu^{3+} ions are well-known commercial red phosphors. Recently, an anomalous thermalization phenomenon due to restricted phonon relaxation has been observed in Eu^{3+}/Gd_2O_3 nanotubes.[5] Eu^{3+}/Gd_2O_3 nanophosphors have also been used as fluorescent markers in a variety of immunosensing application.[6,7] The use of upconverting nanophosphors of Gd_2O_3 doped with Er^{3+} or Sm^{3+} as biolabels for immunoassays is stimulating even more interest since they possess distinct advantages such as the absence of the autofluorescence of biomolecules and no need for time-resolved detection compared to commonly used down-converting phosphors.[8] Furthermore, since Gd^{3+} is a known contrast agent for magnetic resonance imaging (MRI), RE-doped Gd_2O_3 nanophosphors may function as both fluorescence and MRI labels.[8] Despite the promising prospect of RE-doped Gd_2O_3 nanophosphors, their optical behaviors, particularly, the excited-state dynamics of RE ions, have received little attention. Most of the previous work on $Er^{3+}(Yb^{3+})/Gd_2O_3$ nanophosphors was focused on material synthesis, characterization, or an upconversion mechanism.[9−12] To date, temperature dependence of the luminescence decay from the thermalized states ($^2H_{11/2}$ and $^4S_{3/2}$) and vibronic side bands in the excitation spectra of Er^{3+}/Gd_2O_3 crystals have not been thoroughly investigated. A clear understanding of these aspects, however, is essential for the development of novel biolabels and nanosensors based on Er^{3+}/Gd_2O_3 nanophosphors with high luminescence efficiency.

In this paper, spectroscopic properties, particularly, the excited-state dynamics of Er^{3+} in 40−50 nm Gd_2O_3 nanocrystals, are investigated based on laser- or xenon-excited spectroscopic experiments. The temperature-dependent lifetime of the green emission from the $^4S_{3/2}$ state, which is thermally coupled to the upper state of $^2H_{11/2}$, is experimentally determined by utilizing the efficient energy transfer between Gd^{3+} and Er^{3+}. Unusual phonon side bands with fine structures in the low-temperature excitation spectra of Er^{3+} have been observed in Gd_2O_3 nanocrystals and analyzed for the first time.

2. Experimental Section

The cubic Er^{3+}/Gd_2O_3 (1 atom %) nanocrystals used in this study were prepared by a simple sol−gel method. A detailed description of the preparation and characterization of the nanocrystals has been reported by Guo et al.[9−11] For comparison purposes, cubic submicron counterparts (hereafter referred to as bulk counterparts) with the same composition were prepared by annealing the as-prepared nanoparticles in air at 850−950 °C for about 12 h. The morphology of the sample was characterized by a JEOL-2010 transmission electron microscope (TEM) and a JSM6700F field-emission scanning electron

* To whom correspondence should be addressed. Phone and fax: +86-591-8764-2575. E-mail: xchen@fjirsm.ac.cn.
† Chinese Academy of Sciences.
‡ Argonne National Laboratory.
§ University of Science and Technology of China.

10.1021/jp066223e CCC: $37.00
Published on Web 06/15/2007

microscopy (SEM). The powder X-ray diffraction pattern (XRD) of the samples was measured by an X-ray diffractometer (PANalytical X'Pert PRO) with Cu $K\alpha_1$ radiation.

Emission and excitation spectra and transient decays were recorded on an Edinburgh Instruments FLS920 spectrofluorimeter equipped with both continuous (450W) xenon and pulsed xenon or hydrogen lamps. For low-temperature measurements, samples were mounted on a closed cycle cryostat (10−350 K, DE202, Advanced Research Systems). Laser spectroscopic experiments were performed at Argonne. The sample was mounted on an Optistat bath cryostat (Oxford Instruments, 2−350 K). A pulsed dye laser (Lambda Physik, Scanmate 2EC), which provides a pulse width of 5 ns, a repetition rate of 10 Hz, and a tunable range from 480 to 540 nm, was used to pump the samples. The fluorescence was dispersed by a 1 m monochromator (SPEX 1704) and detected with a cooled RCA C31034 photomultiplier. The signals were recorded using a gated boxcar (Stanford Research Systems, model SR250). All spectra were corrected for the intensities as well as the line positions.

3. Results and Discussion

TEM and SEM images (Figure S1 in Supporting Information) show that the size distribution of Er^{3+}/Gd_2O_3 nanocrystals is broad, with an average size of 40−50 nm, and the nanoparticles tend to aggregate. For comparison, the particle size of the submicron counterparts is approximately 110−130 nm. The XRD patterns of both nanocrystals and bulk counterparts (Figure S2, Supporting Information) can be exclusively indexed as the cubic Gd_2O_3 phase (JCPDS #86-2477, space group $Ia\bar{3}$), and no trace of characteristic peaks were observed for other impurity phases such as monoclinic Gd_2O_3 or erbium oxides. By means of the Debye−Scherrer equation, the average size of the nanocrystals is estimated to be approximately 41 nm,[9,10] in accordance with the observations of TEM and SEM.

3.1. Reciprocity Relation Between the Excitation and Emission Spectra. Figure 1a shows the room-temperature (RT) green emission of Er^{3+}/Gd_2O_3 nanocrystals under the excitation at 379.65 nm, which corresponds to the $^4I_{15/2} \rightarrow {}^4G_{11/2}$ transition. Figure 1b shows the RT excitation spectrum in the region of the $^4I_{15/2} \rightarrow {}^2H_{11/2}$ transition by monitoring the strongest emission line of the $^4S_{3/2} \rightarrow {}^4I_{15/2}$ transition at 563.7 nm. On the basis of the high-resolution excitation and emission spectra at 10 and 295 K, we have identified the crystal-field (CF) levels below 43000 cm^{-1} for Er^{3+} in the C_2 sites of Gd_2O_3. Further CF level fitting and Judd−Ofelt intensity calculations are in progress. It should be noted that the CF environment of Er^{3+} in Gd_2O_3 is found to be almost the same as that in the Y_2O_3 or Er_2O_3 host due to very similar crystal structures.[13,14] For comparison, the line pattern in Figure 1a is similar to that of Er^{3+}/Y_2O_3 crystals.[15−17] More than 30 lines are identified, and most of them are labeled in Figure 1a. The observed luminescence lifetimes of transitions from the $^2H_{11/2}$ or $^4S_{3/2}$ states have the same value because of the thermal equilibrium between the two states. The emission lines from the $^2H_{11/2}$ state are not observed below 170 K due to a negligibly small population. Consistently, all emission lines from the $^2H_{11/2}$ state are also observed in the RT excitation spectrum (Figure 1b), indicating a possible reciprocity relationship between them. The reciprocity method based on the McCumber theory is generally a very powerful tool for the evaluation of RE laser crystals, which permits one to calculate the emission cross sections if the absorption cross section is known from measurement (or vice versa).[18,19] It is demonstrated that the reciprocity relation remains also valid for the broad transition bands of RE-doped glass.[20,21] For transitions between two multiplets, the emission cross section may be expressed as[19]

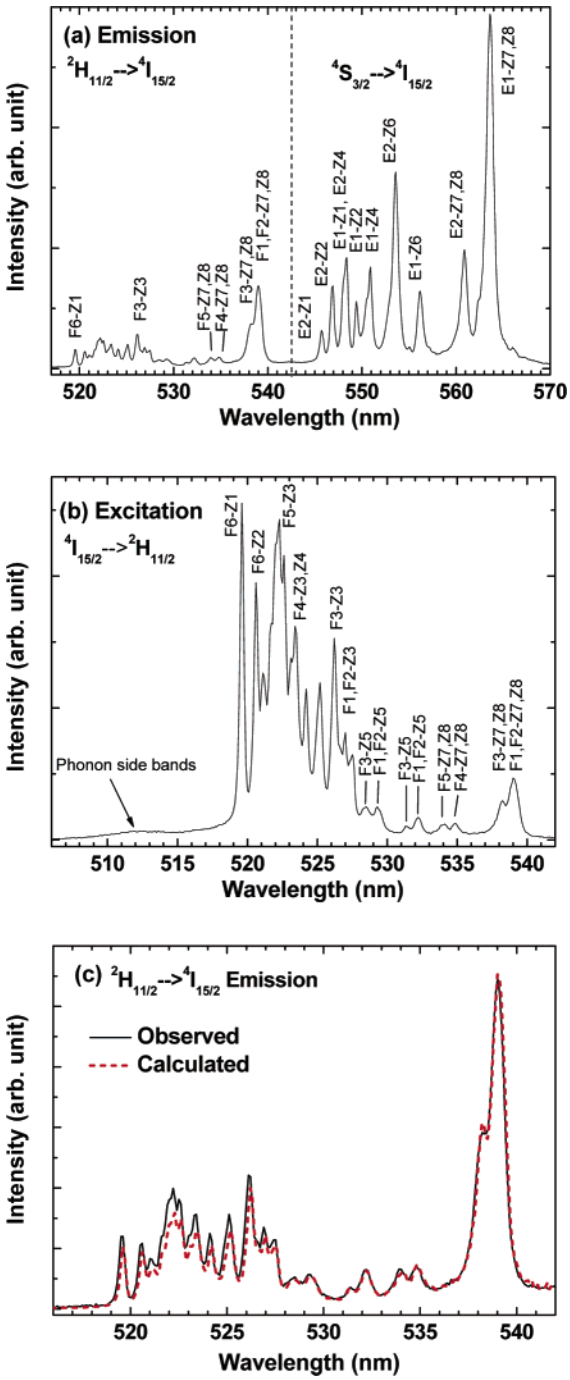

Figure 1. (a) RT emission spectrum from the thermally coupled $^2H_{11/2}$ and $^4S_{3/2}$ to the $^4I_{15/2}$ of Er^{3+} in Gd_2O_3 nanocrystals excited at 379.65 nm; (b) RT excitation spectrum in the region of $^4I_{15/2} \rightarrow {}^2H_{11/2}$, monitoring the $^4S_{3/2} \rightarrow {}^4I_{15/2}$ emission at 563.7 nm; (c) comparison of the calculated and observed emission spectra for the $^2H_{11/2} \rightarrow {}^4I_{15/2}$ transition. F, E, and Z represent $^2H_{11/2}$, $^4S_{3/2}$, and $^4I_{15/2}$, respectively, and the CF levels of them (in units of cm^{-1}) were experimentally determined to be 19048 (F1), 19055 (F2), 19081 (F3), 19196 (F4), 19227 (F5), and 19250 (F6); 18240 (E1) and 18326 (E2); and 0 (Z1), 38 (Z2), 76 (Z3), 87 (Z4), 159 (Z5), 258 (Z6), 487 (Z7), and 500 (Z8). In (a), the emissions from the $^2H_{11/2}$ and $^4S_{3/2}$ states are separated by a dashed line, and the left part is enlarged in (c). In (c), the dashed line denotes the calculated emission spectrum based on the reciprocity method, which has been normalized at the observed line intensity at 538.7 nm.

$$\sigma_{em}(\nu) = \sigma_{abs}(\nu)\frac{Z_l}{Z_u}\exp\left(\frac{E_{ZL} - h\nu}{kT}\right) \quad (1)$$

where E_{ZL} refers to the energy gap between the lowest CF levels of the upper and lower multiplets, and Z_l (or Z_u) is the partition function of the lower (or upper) state. Assuming that the excitation intensity is proportional to its absorption cross section, the $^2H_{11/2} \rightarrow {}^4I_{15/2}$ emission spectrum can be calculated from the observed excitation spectrum of the $^4I_{15/2} \rightarrow {}^2H_{11/2}$ transition using eq 1. As shown in Figure 1c, the calculated emission spectrum is in excellent agreement with the observed one, even for the very fine structures, which unambiguously confirms the validity of the reciprocity method in relating the emission and excitation spectra. The assumption that the excitation intensity is proportional to its absorption cross section holds only for the excitation to those levels that are followed by a very fast nonradiative relaxation to the monitored level (for example, excitation to the $^4F_{7/2,5/2,3/2}$ and $^2H_{11}$ states by monitoring the emission from the $^4S_{3/2}$ state of Er^{3+}). The above extension of the reciprocity method is very useful to derive the emission or excitation spectra that are difficult to be experimentally measured, due to some reasons, for RE-doped bulk crystals or nanocrystals.

3.2. Luminescence Dynamics. The luminescence decays of the $^4S_{3/2}$ state in Er^{3+}/Gd_2O_3 nanocrystals and the bulk counterparts have been measured at different temperatures (10−297 K). It is expected that the luminescence of Er^{3+} ions from the $^4S_{3/2}$ state exhibits a single-exponential decay in a highly diluted host (in this case, the nominal concentration is only 1 atom %) due to the lack of energy-transfer (ET) processes such as self-quenching cross relaxation.[16,22] In fact, our results show that the bulk counterparts exhibit nearly single-exponential decays at different temperatures (Figure S4, Supporting Information), whereas the decay curves for the $^4S_{3/2}$ state of Er^{3+} in the nanocrystals deviate significantly from a single exponential when excited directly to the thermally coupled state of $^2H_{11/2}$. It is evident that there exists an ET process from Er^{3+} to the acceptors or traps (for example, surface defects) in nanocrystals. Capobianco et al. observed the similar deviation from single-exponential decay and a much shorter lifetime than in the bulk upon a 488 nm laser excitation in $Er^{3+}(Yb^{3+})/Y_2O_3$ nanocrystals with a high doping concentration.[16,22] It is difficult to accurately extract the intrinsic lifetime (τ) of the $^4S_{3/2}$ state from those curves shown in Figure 2. Here, we have developed an approach in order to experimentally determine the intrinsic lifetime of $^4S_{3/2}$. The excitation spectrum in the ultraviolet region clearly indicates a much more efficient ET from Gd^{3+} to Er^{3+} in the nanocrystals than that in the bulk counterparts under the excitation to the ^6I state of Gd^{3+} (Figure S3, Supporting Information). As a result, the depopulation of $^4S_{3/2}$ due to the ET from Er^{3+} to the acceptors or traps in the nanocrystals can be completely offset by the more efficient feeding due to the ET from the $^6P_{7/2}$ of Gd^{3+} to the $^2P_{3/2}$ of Er^{3+} followed by nonradiative and radiative relaxation to $^4S_{3/2}$. Note that such enhanced ET from Gd^{3+} to Er^{3+} ions in the nanocrystals has not been reported before. Figure 3 shows the observed luminescence decays of the $^4S_{3/2}$ state at various temperatures under the excitation to the ^6I state of Gd^{3+} at 275.32 nm. The energy level diagrams of Er^{3+} and Gd^{3+} ions as well as the ET path between them are schematically plotted in Figure 4. Different from those in Figure 2, each curve in Figure 3 exhibits a rising edge at the initial stage and a single-exponential decay in the tail. Thus, the intrinsic lifetimes of $^4S_{3/2}$ from 10 to 297 K can be determined from the tails, as presented in Figure 5 (see also Table S1, Supporting Information). The lifetimes of $^4S_{3/2}$ for

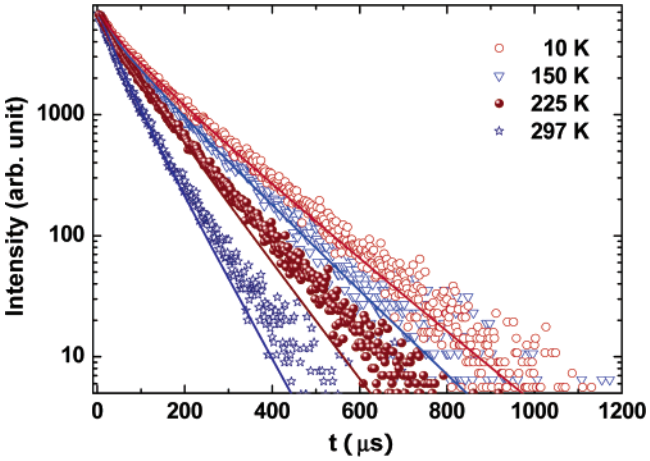

Figure 2. Luminescence decays of the $^4S_{3/2}$ state in Er^{3+}/Gd_2O_3 nanocrystals at various temperatures when directly pumping to the $^2H_{11/2}$ at 519.6 nm and monitoring the $^4S_{3/2} \rightarrow {}^4I_{15/2}$ emission at 563.7 nm. Four typical curves at 10, 150, 225, and 297 K are shown. The scattering points are experimental, and the solid curves are the fitting results according to the Inokuti−Hirayama model.

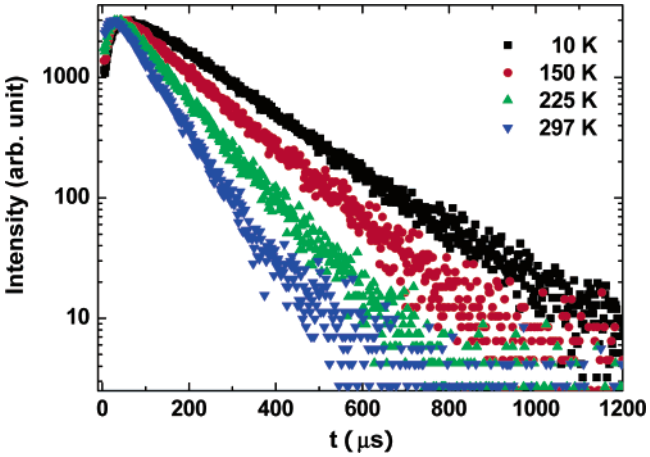

Figure 3. Luminescence decays of the $^4S_{3/2}$ state in Er^{3+}/Gd_2O_3 nanocrystals at various temperatures when pumping to the ^6I state of Gd^{3+} at 275.32 nm and monitoring the $^4S_{3/2} \rightarrow {}^4I_{15/2}$ emission at 563.7 nm. Four typical curves at 10, 150, 225 and 297 K are shown.

Er^{3+} in the nanocrystals (165 and 74 μs, respectively, at 10 and 297 K) is somewhat shorter than those in the bulk counterparts (186 and 84 μs at 10 and 297 K) but comparable to the Er/Y_2O_3 crystals (155 μs at 77K and 88 μs at 296 K).[23] The lifetime shortening in the nanocrystals may be caused by the increasing multiphonon relaxation, owing to the presence of surface defects in the nanocrystals.

Once the intrinsic lifetime of $^4S_{3/2}$ was obtained, we were able to fit the nonexponential decays in Figure 2 by the Inokuti−Hirayama model based on the electric dipole−dipole interaction between donor and acceptor, which is given by $I(t) = I_0 \exp[-t/\tau - C(t/\tau)^{1/2}]$.[24] The good agreement between the observed and fitted decays at various temperatures is shown in Figure 2, indicating the success of the Inokuti−Hirayama model. The ET rate extracted from the fitted C parameter was found to be not very sensitive to temperature until RT was approached. As depicted in Figure 4, the appearance of a rise time in Figure 3 is due to the ET from the $^6P_{7/2}$ of Gd^{3+} to the $^2P_{3/2}$ of Er^{3+} followed by the nonradiative and radiative relaxation to the $^4S_{3/2}$ state of Er^{3+}, which prevails against the other ET processes from the Er^{3+} ions to traps in the nanocrystals. As shown in Figure 3, the rise time increases as the temperature decreases (66 μs at

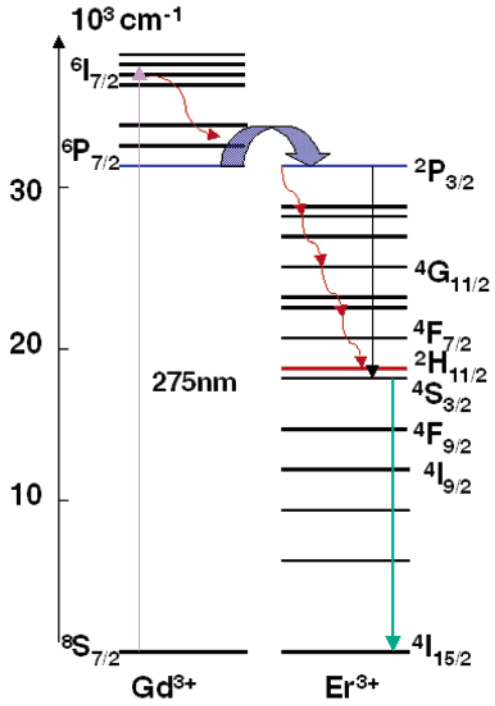

Figure 4. Schematic energy-transfer mechanism between Er^{3+} and Gd^{3+} ions in Er^{3+}/Gd_2O_3 nanocrystals.

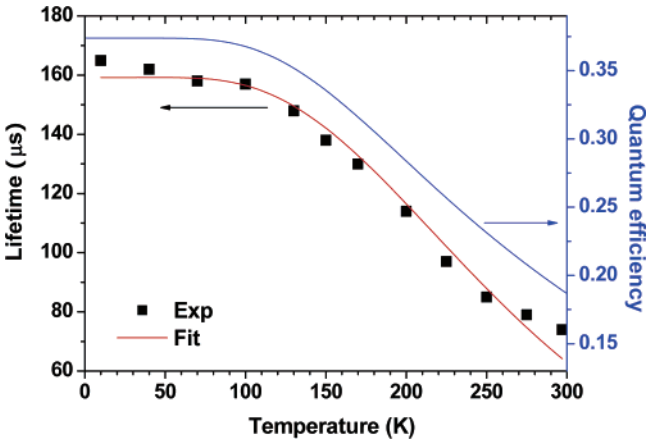

Figure 5. The intrinsic luminescence lifetime and quantum efficiency of the $^4S_{3/2}$ state in Er^{3+}/Gd_2O_3 nanocrystals at various temperatures.

10 K and 28 μs at 297 K). This trend is in accordance with the lifetime variation of the $^2P_{3/2}$ state of Er^{3+} with the temperature (78 μs at 10 K and 32 μs at 297 K), thus confirming the ET mechanism discussed above.

The common value of the decay time from two thermalized multiplets (3 and 2) can be expressed as[25,26]

$$\tau^{-1} = \frac{g_2A_2 + g_3A_3e^{-\Delta E/kT}}{g_2 + g_3e^{-\Delta E/kT}} \quad (2)$$

where ΔE is the energy difference between levels 3 and 2; g_2 and g_3 and A_2 and A_3 are the degeneracies and total radiative and nonradiative probabilities, respectively, of the levels. Particularly, for $^4S_{3/2}$ (level 2) and $^2H_{11/2}$ (level 3), $g_2 = 4$, $g_3 = 12$, and $\Delta E = 860$ cm^{-1}. It is reasonable to assume that both multiplets have the same temperature-dependent multiphonon relaxation rate. According to the energy gap law, the nonradiative transition rate can be expressed as[23,27]

$$A_{nonrad} = W_0[1 - \exp(-\hbar\omega_{eff}/kT)]^{-(\Delta E0)/(\hbar\omega_{eff})} \quad (3)$$

where $\hbar\omega_{eff}$ is the effective phonon energy of the lattice vibrations involved in the nonradiative relaxation, W_0 is the spontaneous phonon relaxation rate at 0 K, and $\Delta E0$ is the energy gap (2800 cm^{-1}) between $^4S_{3/2}$ and the next low-lying state of $^4F_{9/2}$. Then, the temperature-dependent lifetime of $^4S_{3/2}$ can be approximately expressed as follows

$$\tau^{-1} = \frac{1/\tau_2^{rad} + 3e^{-\Delta E/kT}/\tau_3^{rad}}{1 + 3e^{-\Delta E/kT}} + W_0[1 - \exp(-\hbar\omega_{eff}/kT)]^{-(\Delta E0)/(\hbar\omega_{eff})} \quad (4)$$

Two parts (common radiative rate + multiphonon relaxation rate) contribute to the observed lifetime in eq 4. The radiative lifetimes of $^4S_{3/2}$ and $^2H_{11/2}$ are determined to be 426 and 65 μs, respectively, based on the fitting of three Judd−Ofelt intensity parameters from the RT excitation spectrum and the measured lifetime of the $^4I_{13/2}$ multiplet, which takes into account the CF-induced J-mixing effect. According to this simple model, the parameters of W_0 and ω_{eff} are determined to be 3933 ± 85 s^{-1} and 388 ± 9 cm^{-1} by a fit to the observed lifetimes at various temperatures. The fitting results in Figure 5 are in good agreement with those measured lifetimes from 10 K to RT, which indicates the validity of the above model that we proposed. The parameter of W_0 for Er/Gd_2O_3 is comparable to that for Er/Y_2O_3 crystals (for instance, 5019 s^{-1} at 77 K by Weber[23] and 6500 s^{-1} at 4.2 K by Risebserg and Moos[27]). The effective phonon frequency of 388 cm^{-1} matches one of the main infrared absorption bands at 391 cm^{-1} in Gd_2O_3 crystals.[28] The quantum efficiency, which is equal to the ratio of the radiative transition rate to the total transition rate from the thermally coupled states, is also calculated. As shown in Figure 5, the trend of temperature dependence of the quantum efficiency follows similarly that of the luminescence lifetime, and the quantum efficiency is reduced from 0.374 at 10 K to 0.187 at 300 K. Therefore, the mechanism for the decrease of the $^4S_{3/2}$ lifetime at a higher temperature is primarily attributed to the temperature-dependent nonradiative relaxation from $^4S_{3/2}$ to $^4F_{9/2}$, which involves approximately seven phonons at 388 cm^{-1}. Similarly, as pointed out by Weber for Er^{3+} in Y_2O_3 crystals, thermal population of the $^2H_{11/2}$ multiplet at a higher temperature is insufficient to account for the observed decrease of the common decay time, although the radiative lifetime of $^2H_{11/2}$ (78 μs) is much shorter than that for $^4S_{3/2}$ (698 μs).[23] Alencar et al. reported the exploitation of $Er^{3+}/BaTiO_3$ nanocrystals for temperature sensors using the method of the fluorescence intensity ratio of $^2H_{11/2}$ to $^4S_{3/2}$.[29] The drawback of their method is that it is difficult to accurately measure the intensity ratio since many factors may affect the ratio and the luminescence becomes weaker at higher temperature. It is expected that the accuracy and sensitivity of nanosensors based on the lifetime measurement can be significantly enhanced. By measuring the temperature-dependent lifetime of the $^4S_{3/2}$ state of Er^{3+}/Ln_2O_3 (Ln = Y, Gd) crystals, the nature of the observed high effective temperature inside of the crystals when pumping by lasers at 488 or 978 nm may also be resolved.[12,17] That is, if the observed lifetime at RT is equal to a value expected at a temperature higher than RT, it is quite possibly due to laser heating instead of the lack of low-frequency phonon modes (or anomalous thermalization).[30,31]

3.3. Phonon Side Bands. The phonon side bands in a spectrum of Er^{3+}in Gd_2O_3 crystals are expected to be much (at

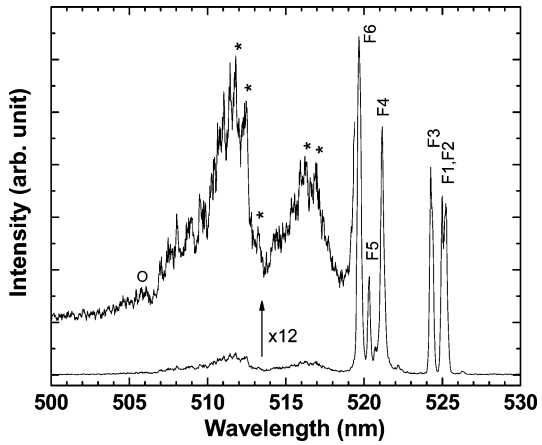

Figure 6. Laser excitation spectrum of Er^{3+}/Gd_2O_3 nanocrystals in the region of $^4I_{15/2} \rightarrow {}^2H_{11/2}$ at 5 K, monitoring the $^4S_{3/2} \rightarrow {}^4I_{15/2}$ emission at 564 nm with a 5 μs gate width and a 12 μs delay from the laser pulse. The ZPLs corresponding to the excitation to the F1−F6 sublevels of $^2H_{11/2}$ are labeled. Phonon side bands are enlarged 12 times for a clear view of the fine structures.

least 1 order of magnitude) weaker than the zero-phonon lines (ZPLs) since it is, in general, regarded as a weak electron−phonon coupling system. However, the stronger-than-expected phonon side bands appear in the laser excitation spectra of the $^4I_{15/2} \rightarrow {}^2H_{11/2}$ transition of Er^{3+} in Gd_2O_3 nanocrystals at 5 K, as shown in Figure 6. The side bands in the high-energy side of the six ZPLs are due to the absorption of a photon plus the spontaneous emission of one phonon. The integrated intensity ratio (R) of the phonon side bands to ZPLs in Figure 6 reaches a value of 0.335. The rich side band structure reflects the density of states of phonon modes that couple to the pure electronic transitions. It is evident that two bands peaking at 511.8 and 516.2 nm correspond to the one-phonon replica of the excitation to CF levels F1−F3 and F4−F6, respectively. As can be seen from the enlarged part in Figure 6, vibronic lines marked by the star signs correspond well to a blue shift of ~298 cm^{-1} of the six ZPLs marked by F1−F6, indicating a coupling with the phonon mode of 298 cm^{-1}. Note that vibronic lines associated with F1 and F2 are too close to be resolved. Besides, the two phonon side bands have very similar fine structures at 5 K and merge into one broad side band at RT due to the appearance of abundant ZPLs (>34 lines in Figure 1b). Two mechanisms known as the Δ and M processes can contribute to the phonon side bands of RE electronic transitions.[32] Electron−phonon coupling with an infrared-active (or ungerade) vibrational modes is typical of the M process, whereas coupling with Raman-active (gerade) lattice modes is typical of the Δ process. The origin of phonon side bands in Figure 6 is mainly due to the M process based on the following evidence. First, the blue-shift energy of 298 cm^{-1} matches the strong absorption of the infrared phonon modes at 302 and 318 cm^{-1}.[28] The highest frequency of the phonon modes involved is around 530 cm^{-1} (see the line marked by a circle in Figure 6), which corresponds to the maximum infrared phonon frequency (535 cm^{-1}).[28] By contrast, one phonon replicas coupling with the strongest Raman-active mode[11] with a frequency of 360 cm^{-1} are not observed. Second, similar phonon side bands are also observed in the excitation to the $^4G_{11/2}$ multiplet. Both transitions from $^4I_{15/2}$ to $^2H_{11/2}$ and $^4G_{11/2}$ are hypersensitive, with large rank-2-reduced matrix elements of the unit tensor. It thus results in enhanced vibronic side bands via an admixture of opposite parity, according to the theory of M-process vibronic transition probability by Judd and Blasse.[32−34] It should be noted that the above phonon side bands are also observed in the excitation spectra by a Xe lamp. However, the intensity ratio R (0.105) is only about one-third of that by laser excitation, which indicates that the intensity of phonon side bands is closely related to the excitation power. Currently, it is not clear to us why and how the phonon side bands are related to the excitation power.

4. Conclusions

The excited-state dynamics of Er^{3+} (1 atom %) in 40−50 nm Gd_2O_3 nanocrystals has been investigated using laser and xenon excitation in spectroscopic experiments, along with theoretical analyses. The RT emission and excitation spectra between the $^2H_{11/2}$ and $^4I_{15/2}$ transition obey an excellent reciprocity relationship predicted by the McCumber theory. The luminescence decay from the $^4S_{3/2}$ multiplet of Er^{3+} in the nanocrystals shows nonexponential characteristics when excited directly to the thermally coupled $^2H_{11/2}$ multiplet with temperatures varying from 10 to 300 K. This effect is attributed to energy transfer to defects in the nanocrystals. The nonexponential decays can be well fitted by the Inokuti−Hirayama model in terms of electric dipole−dipole interaction between the donor and acceptor. It turns out that the population feeding from Gd^{3+} to Er^{3+} is efficient enough to overwhelm the ET of Er^{3+} in the $^4S_{3/2}$ emitting state to ions at defect sites. As a result, when excited to the ^6I states of Gd^{3+} (275 nm), the $^4S_{3/2}$ decay exhibits a significant rise time followed by an exponential tail. The temperature dependence of the observed lifetimes of the $^4S_{3/2}$ multiplet has been well interpreted by a simple model, which takes into account the contributions from both multiphonon transition and the thermally coupled levels of $^2H_{11/2}$. The calculated quantum efficiencies at various temperatures suggest that the change of lifetime of $^4S_{3/2}$ with the temperature is predominantly influenced by the multiphonon transition process to the next low-lying multiplet. Unusually strong phonon side bands with rich structures in the excitation spectra of Er^{3+} have been observed in Gd_2O_3 nanocrystals for hypersensitive transitions. The nature of the phonon side bands is ascribed to the vibrationally induced forced electric dipole transition (M process), which couples to the infrared-active lattice modes.

Acknowledgment. This work was supported by the One Hundred Talents Program from the Chinese Academy of Sciences, the National Natural Science Foundation of China (No. 10504032), the Startup Foundation from the State Ministry of Personnel of China, and the Talent Youth Foundation of Fujian Province of China (No. 2006F3137). Work at Argonne National Laboratory was supported by the U.S. Department of Energy, Office of Basic Energy Sciences, Division of Chemical Sciences, Geosciences, and Biosciences, under Contract DE-AC02-06CH11357.

Supporting Information Available: TEM, SEM, and XRD of Er^{3+}/Gd_2O_3 nanocrystals and bulk counterparts; room-temperature excitation spectra in the ultraviolet region for Er^{3+} ions in the nanocrystals and bulk counterparts; luminescence decays of the $^4S_{3/2}$ state in bulk counterparts at various temperatures when directly excited to the $^2H_{11/2}$; comparison of the luminescence lifetime of the $^4S_{3/2}$ state of Er^{3+} in the nanocrystals and bulk counterparts. This material is available free of charge via the Internet at http://pubs.acs.org.

References and Notes

(1) Tanner, P. A. *J. Nanosci. Nanotech.* **2005**, *5*, 1455.
(2) Tissue, B. M. *Chem. Mater.* **1998**, *10*, 2837.

(3) Liu, G. K.; Chen, X. Y. Spectroscopic Properties of Lanthanides in Nanomaterials. In *Handbook on the Physics and Chemistry of Rare Earths*; Gschneidner, K. A., Jr., Bunzli, J. C. G., Pecharsky, V. K., Eds.; North-Holland: Amsterdam, The Netherlands, 2007; Vol. 37; Chapter 233, p 99.

(4) Gordon, W. O.; Carter, J. A.; Tissue, B. M. *J. Lumin.* **2004**, *108*, 339.

(5) Liu, L. Q.; Ma, E.; Li, R. F.; Liu, G. K.; Chen, X. Y. *Nanotechnology* **2007**, *18*, 015403.

(6) Nichkova, M.; Dosev, D.; Gee, S. J.; Hammock, B. D.; Kennedy, I. M. *Anal. Chem.* **2005**, *77*, 6864.

(7) Nichkova, M.; Dosev, D.; Perron, R.; Gee, S. J.; Hammock, B. D.; Kennedy, I. M. *Anal. Bioanal. Chem.* **2006**, *384*, 631.

(8) Dosev, D.; Kennedy, I. M.; Godlewski, M.; Gryczynski, I.; Tomsia, K.; Goldys, E. M. *Appl. Phys. Lett.* **2006**, *88*, 011906.

(9) Guo, H.; Dong, N.; Yin, M.; Zhang, W. P.; Lou, L. R.; Xia, S. D. *J. Phys. Chem. B* **2004**, *108*, 19205.

(10) Guo, H.; Li, Y. F.; Wang, D. Y.; Zhang, W. P.; Yin, M.; Lou, L. R.; Xia, S. D. *J. Alloys Compd.* **2004**, *376*, 23.

(11) Guo, H.; Zhang, W. P.; Yin, M.; Lou, L. R.; Xia, S. D. *J. Rare Earths* **2004**, *22*, 365.

(12) Lei, Y. Q.; Song, H. W.; Yang, L. M.; Yu, L. X.; Liu, Z. X.; Pan, G. H.; Bai, X.; Fan, L. B. *J. Chem. Phys.* **2005**, *123*, 174710.

(13) Gruber, J. B.; Henderson, J. R.; Muramoto, M.; Rajnak, K.; Conway, J. G. *J. Chem. Phys.* **1966**, *45*, 477.

(14) Kisliuk, P.; Krupke, W. F. *J. Chem. Phys.* **1964**, *40*, 3606.

(15) Capobianco, J. A.; Vetrone, F.; Boyer, J. C.; Speghini, A.; Bettinelli, M. *J. Phys. Chem. B* **2002**, *106*, 1181.

(16) Capobianco, J. A.; Vetrone, F.; D'Alesio, T.; Tessari, G.; Speghini, A.; Bettinelli, M. *Phys. Chem. Chem. Phys.* **2000**, *2*, 3203.

(17) Tanner, P. A.; Wong, K. L. *J. Phys. Chem. B* **2004**, *108*, 136.

(18) McCumber, D. E. *Phys. Rev.* **1964**, *136*, A954.

(19) Payne, S. A.; Chase, L. L.; Smith, L. K.; Kway, W. L.; Krupke, W. F. *IEEE J. Quantum Electron.* **1992**, *28*, 2619.

(20) Martin, R. M.; Quimby, R. S. *J. Opt. Soc. Am. B* **2006**, *23*, 1770.

(21) Quimby, R. S. *J. Appl. Phys.* **2002**, *92*, 180.

(22) Vetrone, F.; Boyer, J. C.; Capobianco, J. A.; Speghini, A.; Bettinelli, M. *J. Appl. Phys.* **2004**, *96*, 661.

(23) Weber, M. J. *Phys. Rev.* **1968**, *171*, 283.

(24) Inokuti, M.; Hirayama, F. *J. Chem. Phys.* **1965**, *43*, 1978.

(25) Di Bartolo, B. *Optical Interactions in Solids*; John Wiley & Sons, Inc.: New York, 1968.

(26) Liu, G. K.; Chen, X. Y.; Huang, J. *Mol. Phys.* **2003**, *101*, 1029.

(27) Riseberg, L. A.; Moos, H. W. *Phys. Rev.* **1968**, *174*, 429.

(28) McDevitt, N. T.; Davidson, A. D. *J. Opt. Soc. Am.* **1966**, *56*, 636.

(29) Alencar, M. A. R. C.; Maciel, G. S.; de Araujo, C. B.; Patra, A. *Appl. Phys. Lett.* **2004**, *84*, 4753.

(30) Liu, G. K.; Chen, X. Y.; Zhuang, H. Z.; Li, S.; Niedbala, R. S. *J. Solid State Chem.* **2003**, *171*, 123.

(31) Liu, G. K.; Zhuang, H. Z.; Chen, X. Y. *Nano Lett.* **2002**, *2*, 535.

(32) Meijerink, A.; Donega, C. D.; Ellens, A.; Sytsma, J.; Blasse, G. *J. Lumin.* **1994**, *58*, 26.

(33) Blasse, G. *Int. Rev. Phys. Chem.* **1992**, *11*, 71.

(34) Judd, B. R. *Phys. Scr.* **1980**, *21*, 543.